Journal of Materials Chemistry

Cite this: J. Mater. Chem., 2012, 22, 17183

www.rsc.org/materials

PAPER

Improvement of the hydrogen storage kinetics of $NaAlH_4$ with Ti-loaded high-ordered mesoporous carbons (Ti-OMCs) by melt infiltration†

Renjin Xiong, Ge Sang,* Xiayan Yan, Guanghui Zhang and Xiaoqiu Ye

Received 29th March 2012, Accepted 18th June 2012
DOI: 10.1039/c2jm31961f

Combination of nanoconfinement and catalyst addition is a promising strategy to enhance the kinetics and reversibility of hydrogen storage in complex hydrides. Herein, Ti-loaded high-ordered mesoporous carbons (Ti-OMCs) were directly synthesized *via* a solvent evaporation induced self-assembly method (EISA) with *in situ* crystallization and carbonation technology using phenolic resols, tetrabutyl titanate ($Ti(OBu)_4$) and triblock copolymer F127 as organic carbon sources, Ti sources and templates, respectively. The obtained Ti-OMCs exhibit uniform pore sizes (4 nm), high specific surface area (427.9 $m^2\ g^{-1}$) and large pore volumes (0.34 $cm^3\ g^{-1}$), which were used to combine catalyst addition and nanoconfinement to improve the hydrogen storage properties of $NaAlH_4$ by melt infiltration. The hydrogen desorption curves show that $NaAlH_4$ with Ti-OMCs exhibits better kinetic properties than both nanocrystalline TiO_2 catalysed $NaAlH_4$ and melt-infiltrated $NaAlH_4$ with high ordered mesoporous carbons (OMCs). The hydrogen-release onset temperature of $NaAlH_4$ with Ti-OMCs is reduced to less than 60 °C, and 80% hydrogen is released in less than 20 min. In addition, $NaAlH_4$ with Ti-OMCs exhibit good reversibility and cycling stability, and the optimum rehydrogention temperature is 120 °C.

1. Introduction

Hydrogen is considered a promising alternative energy carrier that can potentially facilitate the transition from fossil fuels to sources of clean energy because it is the most abundant element in the universe, contains the highest energy density per unit mass (142 MJ kg^{-1}) and has a low environmental impact.[1–4] However, one of the most difficult remaining technological issues for the conversion from fossil fuels to a "hydrogen economy" is to develop solid hydrogen storage systems.[4–6] Many materials have been developed, including metal–organic frameworks,[7] nanoporous polymers,[8] carbon-based materials,[9] metal hydrides (such as MgH_2)[10] and intermetallic alloys (such as $LaNi_5$).[11] Despite decades of extensive efforts, no material has been found which can effectively combine high gravimetric density, safety, low cost and fast hydrogen release and uptake kinetics. Recently, complex hydrides (such as $NaAlH_4$, $LiAlH_4$ and $LiBH_4$) have been considered as one of the most promising materials for hydrogen storage due to their potentially high gravimetric capacities, as well as their ability to be engineered for favorable hydrogen release kinetics.[12–15] Among the complex hydrides, $NaAlH_4$ has been widely studied after the pioneering research by Bogdanovic and Schwickardi[16] because of its relative large hydrogen storage capacity (5.6 wt%) and moderate temperature for reversible hydrogen release/uptake according to the following two-step reaction:

$$NaAlH_4 \rightleftharpoons {}^1/_3\ Na_3AlH_6 + {}^2/_3\ Al + H_2 \quad (1)$$

$${}^1/_3\ Na_3AlH_6 \rightleftharpoons NaH + {}^1/_3\ Al + \tfrac{1}{2}H_2 \quad (2)$$

The enthalpies (ΔH_d) for hydrogen release in (1) and (2) are 37 and 47 kJ mol^{-1} H_2, respectively, corresponding to the equilibrium temperatures (T_{eq}) = 30 and 100 °C at $p(H_2)$ = 1 bar using the van't Hoff equation, respectively.[17] However, $NaAlH_4$ suffers from inherent limitations as a hydrogen storage media due to low kinetics and poor reversibility.[18–20] Results from extensive research on $NaAlH_4$ have shown that kinetics and reversibility can be improved by doping minor amounts of transition-metal compounds *via* ball milling, using compounds such as $TiCl_3$, TiO_2, $ScCl_3$, $CeAl_2$, $CeCl_3$, K_2TiF_6 and TiB_2.[21–24] Unfortunately, the catalysis mechanism of Ti in $NaAlH_4$ remains unconfirmed after 15 years of investigation.[25] In addition, nanoconfinement of $NaAlH_4$ is another alternative approach to enhance the kinetics and reversibility of $NaAlH_4$ because the physics and chemistry of matter at the nanoscale can be fundamentally altered, for example, the large surface area of the reactants, nanoscale diffusion distances and increased number of atoms in the grain boundaries.[26–29] Nanoconfined $NaAlH_4$ is generally achieved by confining it into nanoporous scaffolds by melt infiltration at high

Science and Technology on Surface Physics and Chemistry Laboratory, Mianyang, 621907, China. E-mail: xrj902@yahoo.com.cn; Fax: +86 0816 3626738; Tel: +86 0816 3626740

† Electronic supplementary information (ESI) available. See DOI: 10.1039/c2jm31961f

hydrogen pressure, using the nanoporous materials such as mesoporous silica (SBA-15),[30] mesoporous carbon (MC)[31] and metal-organic frameworks (MOF).[32]

Very recently, Ngene *et al.* demonstrated that the nanoconfinement of $LiBH_4$ in nanoporous carbon with the addition of Ni by melt infiltration can obviously improve the kinetics of $LiBH_4$ compared to bulk $LiBH_4$, and the Ni addition significantly enhanced the subsequent uptake kinetics of hydrogen under mild conditions.[33] Nielsen *et al.* reported that the hydrogen-release onset temperature of $NaAlH_4$, which was melt-infiltrated in an aerogel doped with 3.0 wt% $TiCl_3$ nanoparticles, was reduced to 33 °C.[34] In a previous study,[35] we have reported an alternative approach to combine catalyst addition (TiO_2 nanoparticles) and nanoconfinement in order to improve the kinetics of $NaAlH_4$ by depositing it on the surface of nanocrystalline titanium dioxide loaded carbon spheres (Ti-CSs). We were able to report that nanoconfined $NaAlH_4$ begins to release hydrogen at approximately 40 °C and releases ~25% of the hydrogen content during heating to 60 °C. Thus, these results indicate that combination of nanoconfinement and catalyst addition is a promising strategy to enhance the kinetics and reversibility of hydrogen storage in complex hydrides.

Herein, we report a simple method to synthesize Ti loaded mesoporous carbons (Ti-OMCs) which can be used to combine catalyst addition and nanoconfinement to improve the kinetics and reversibility of $NaAlH_4$ by melt infiltration. Firstly, Ti-OMCs were directly prepared by a solvent evaporation induced self-assembly method (EISA) with *in situ* crystallization and carbonation technology using phenolic resols, tetrabutyl titanate ($Ti(OBu)_4$) and triblock copolymer F127 as organic carbon sources, Ti sources and templates, respectively. Then $NaAlH_4$ was confined into Ti-OMCs by melt infiltration, and the hydrogen desorption/absorption kinetics and cycling stability were tested on a Sieverts-type apparatus.

2. Experimental

2.1. Chemicals

Pluronic F127 (triblock copolymer poly(ethylene oxide)-*b*-poly(propylene oxide)-*b*-poly(ethylene oxide), PEO-PPO-PEO, $M_{av} = 12\,600$, Sigma-Aldrich) and $NaAlH_4$ were purchased from Sigma-Aldrich Corp. Tetrabutyl titanate ($Ti(OBu)_4$), phenol, formalin aqueous solution (37 wt%), NaOH, sulphuric acid, acetic acid (HAc) and ethanol were purchased from Chengdu Kelong Chemical Reagent Corp. All chemicals were analytical grade and used as received without further purification.

2.2. Synthesis of Ti-OMCs

A 20 wt% resol ethanolic solution was synthesized according to an established method (details are presented in the ESI†).[36] Ti-loaded high-ordered mesoporous carbons (Ti-OMCs) were prepared *via* a solvent evaporation induced self-assembly method followed by *in situ* crystallization and carbonation technology.[37] For a typical synthesis, 0.2 ml of tetrabutyl titanate ($Ti(OBu)_4$) was added to a clear solution containing 0.1 ml of sulphuric acid and 0.2 ml of acetaldehyde in 10 ml of ethanol. A yellow Ti-sol was obtained after the mixture was stirred vigorously for 1 h at room temperature. Triblock copolymer F127 (5.3 g) was dissolved in 50 ml of anhydrous ethanol. Then 20 ml of 20 wt% resol ethanolic solution and the as-obtained yellow Ti-sol were added slowly into the F127 solution with stirring for 1 h at room temperature. The homogeneous mixture was then transferred into the Petri dishes at 40 °C for 24 h in an oven. After being dried, the films were heated at 100 °C for another 24 h. The as-made products, which formed as orange transparent membranes, were then scraped from the Petri dishes and ground into powders. Subsequently, the powders were calcinated at 900 °C in a tubular furnace under an Ar atmosphere with a rate of approximately 1 °C min^{-1}, and held for 4 h at final temperature. The Ti-loaded high-ordered mesoporous carbons, denoted as Ti-OMCs, were obtained after cooling in the furnace to room temperature. For comparison, high-ordered mesoporous carbons (OMCs) were prepared in a similar way without using $Ti(OBu)_4$.

2.3. Confinement of $NaAlH_4$

A mixture of $NaAlH_4$ and the as-prepared Ti-OMCs with a mass ratio of 1 : 2 was obtained by grinding for 5 min in a mortar and then loading and sealing in a sample cell in an Ar-filled glove box. Melt infiltration was performed using an ultra high pressure gas reaction controller (Advanced Materials Corp., USA) by applying a hydrogen pressure of 128 bar and heating to 185 °C, reaching a pressure of approximately 142 bar. The sample was kept at 185 °C for approximately 1 h, and was then cooled in the furnace to room temperature. The hydrogen pressure change in the system (see Fig. S1†) shows that a fraction of $NaAlH_4$ decomposes at these conditions during melt infiltration. For comparison, a further two samples were prepared. $NaAlH_4$ with OMCs were obtained by a similar method, and ball-milled $NaAlH_4$ with 3 mol% TiO_2 was prepared and used as descibed in the literature.[22]

2.4. Characterization

Small-angle X-ray diffraction (SAXRD) patterns and powder X-ray diffraction (XRD) patterns were recorded on a X'Pert-PRO powder X-ray diffractometer. Transmission electron microscopy (TEM) images were taken with a Tecnai-GF20 electron microscope. The sample for TEM measurement was suspended in ethanol and supported on a carbon-coated copper grid. Nitrogen adsorption–desorption data were measured with a Quantachrome Autosorb-1 analyzer at −196 °C. Prior to the measurement, the samples were first degassed at 200 °C for at least 4 h. The surface areas were calculated by the Brunauer–Emmett–Teller (BET) method. The pore size distributions were derived from the adsorption branches of the isotherms using the Barrett–Joyner–Halenda (BJH) model. The hydrogen desorption/absorption kinetics and consecutive cycling of samples were performed on a gas reaction controller (Advanced Materials Corp., USA). During the experiments, the temperature inside the sample cell was measured, and the measurement range of pressure sensors used for hydrogen desorption and absorption cycling test were 0–20 and 0–200 bar with 0.05% accuracy, respectively. The reversible hydrogen storage capacity was calculated in wt% of $NaAlH_4$ according to the pressure changes in the system during testing.

3. Results and discussion

3.1. Preparation of $NaAlH_4$ with Ti-OMCs

Evidence for the formation of ordered mesostructures is provided by small-angle X-ray diffraction (SAXRD) patterns shown in Fig. 1. The as-obtained OMC and Ti-OMC samples show one diffraction peak around $2\theta = 1°$, which suggests that a mesoporous carbon framework is obtained after carbonization at 900 °C.[38] The TEM image (Fig. 2) shows that the Ti-OMCs have a uniform pore size of about 4–5 nm. In addition, nanocrystalline TiO_2 with anatase and rutile mixed phase should be obtained from the crystallization of $Ti(OBu)_4$ after calcination at 900 °C.[38,39] However, no TiO_2 is observed in either the TEM image or the XRD pattern (Fig. 5) of the Ti-OMCs, which may be due to the low content of Ti in the sample and/or low crystallization. The TiO_2 content is about 3 wt% in the Ti-OMCs composite according to the weight loss of carbonization of resol and crystallization of TiO_2 from $Ti(OBu)_4$ at high temperature.[37]

N_2 adsorption–desorption isotherms and BJH pore size distribution curves of Ti-OMCs and $NaAlH_4$ with Ti-OMCs are shown in Fig. 3. All samples exhibit representative type-IV curves with H_2 hysteresis loops, which are typical of ordered mesoporous materials.[40] The pore-size distribution curves calculated from the adsorption branches show a high mesoporous uniformity, with a pore size of about 4 nm, which is in agreement with the TEM image. In comparison to the as-prepared Ti-OMCs, the BET surface area and BJH total pore volume of $NaAlH_4$ with Ti-OMCs decrease from 427.9 to 81.7 $m^2\ g^{-1}$ and from 0.34 to 0.12 $cm^3\ g^{-1}$, respectively, indicating that the surface area and pore volume become drastically reduced after melt infiltration due to incorporation of $NaAlH_4$ into the pores, which is in agreement with previous studies.[26,31]

3.2. Hydrogen desorption kinetics of $NaAlH_4$ with Ti-OMCs

The hydrogen desorption kinetics of the first desorption cycle at 160 °C under vacuum for $NaAlH_4$ with 3 mol% TiO_2, $NaAlH_4$ with OMCs, and $NaAlH_4$ with Ti-OMCs were studied using a gas reaction controller. The kinetic properties of the samples

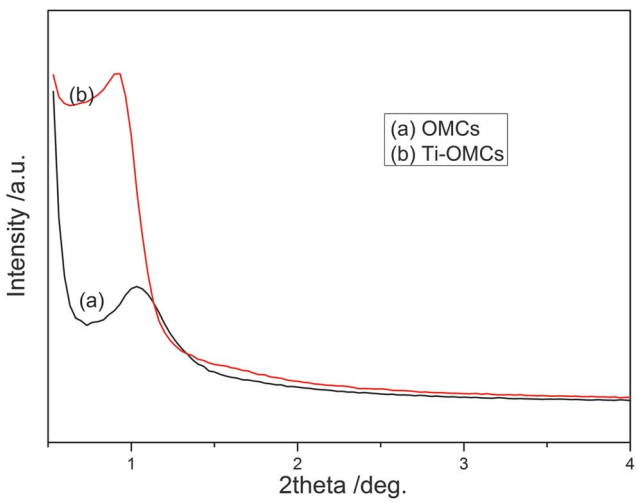

Fig. 1 SAXRD patterns of as-prepared (a) OMCs and (b) Ti-OMCs.

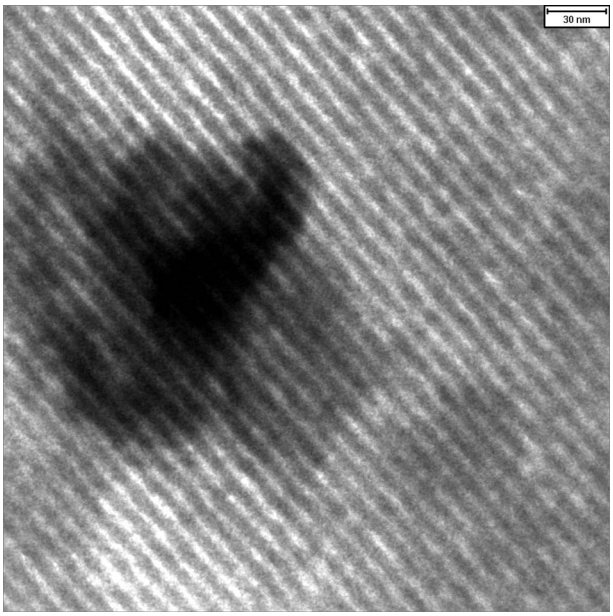

Fig. 2 TEM image of Ti-OMCs.

were compared based on the normalized hydrogen desorption profiles (Fig. 4a). For sample $NaAlH_4$ with 3 mol% TiO_2, hydrogen release begins at approximately 100 °C, and about 63% hydrogen is released in less than 25 min, while the hydrogen desorption rate falls drastically after 25 min and further hydrogen is released in 100 min, indicating that TiO_2 nanoparticles exhibit a good catalytic effect on $NaAlH_4$ for hydrogen storage. The hydrogen desorption of doped-$NaAlH_4$ is completed *via* a two-step reaction corresponding to reactions (1) and (2).[22] For sample $NaAlH_4$ with OMCs, only one hydrogen desorption step is observed from the desorption curve, which is in agreement with previous reports on melt infiltration,[31] and most hydrogen is released after 250 min indicating that the kinetics of the nanoconfined $NaAlH_4$ are much lower than catalyzed $NaAlH_4$. For sample $NaAlH_4$ with Ti-OMCs, the onset hydrogen-release temperature is reduced to less than 60 °C, and most hydrogen is released in about 50 min. In addition, the initial hydrogen desorption stage (inset of Fig. 4a) shows that 80% hydrogen of $NaAlH_4$ with Ti-OMCs is released in less than 20 min during heating to 160 °C, while only about 20 and 40% hydrogen is released during 20 min for samples $NaAlH_4$ with OMCs and $NaAlH_4$ with 3 mol% TiO_2, respectively. Thus, the above results suggest that the order of the efficient improvement of kinetics for $NaAlH_4$ is Ti-OMCs > TiO_2 > OMCs, and we infer that the fastest kinetics properties of $NaAlH_4$ with Ti-OMCs is achieved due to the combination of catalyst addition (TiO_2 nanoparticles) and nanoconfinement for Ti-OMCs by melt infiltration.

In order to verify that hydrogen released from the $NaAlH_4$ with Ti-OMCs composite is due to the nanoconfined $NaAlH_4$ and not Ti-OMCs physical and/or chemical adsorption, hydrogen absorption of a pristine Ti-OMCs composite was carried out at 120 °C and $p(H_2) = 100$ bar, which were the same as the rehydrogenation conditions of $NaAlH_4$ with Ti-OMCs. However, we did not find any obvious hydrogen pressure increases at 160 °C over the course of 17 h (Fig. 4b), indicating

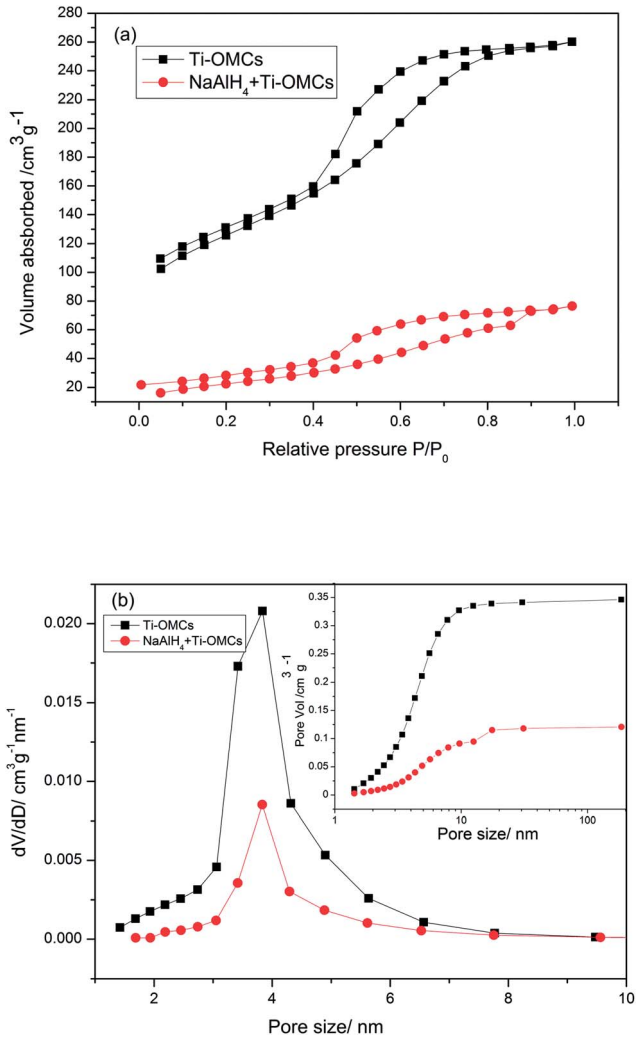

Fig. 3 (a) Nitrogen sorption isotherms, (b) BJH pores size distribution of Ti-OMCs and $NaAlH_4$ with Ti-OMCs. The inset shows the corresponding BJH cumulative volumes determined from the adsorption branch of the isotherms.

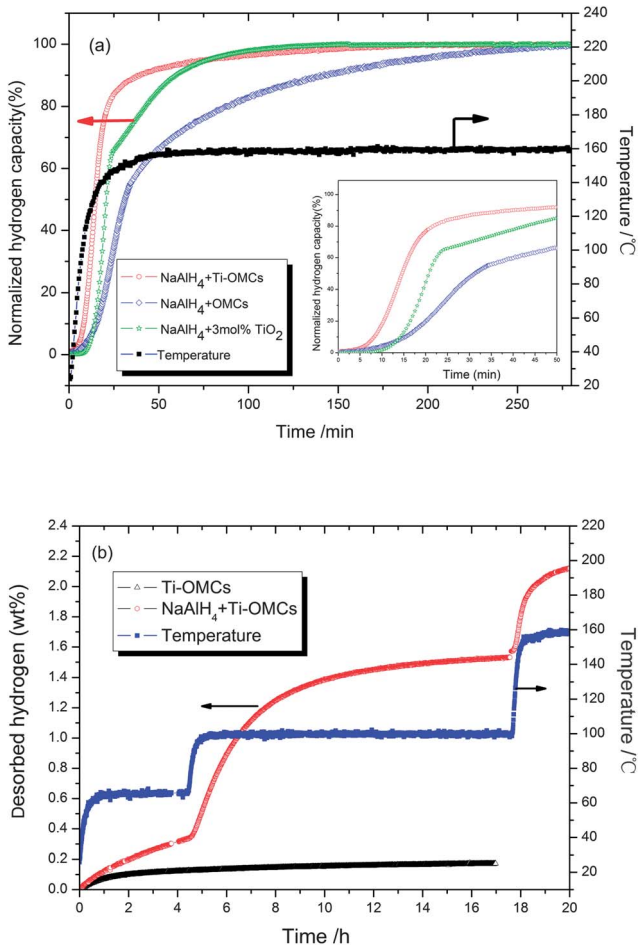

Fig. 4 (a) Normalized hydrogen desorption curves at the first desorption cycle at 160 °C under vacuum for $NaAlH_4$ with 3 mol% TiO_2, $NaAlH_4$ with OMCs, and $NaAlH_4$ with Ti-OMCs, the inset shows the initial desorption stage of samples; (b) hydrogen desorption curves of pristine Ti-OMCs and $NaAlH_4$ with Ti-OMCs at fixed temperatures of 60, 100 and 160 °C.

that pristine Ti-OMCs do not rehydrogenate at these conditions and the released hydrogen originates from the confined $NaAlH_4$. Additionally, in order to further investigate the low temperature kinetic properties of $NaAlH_4$ with Ti-OMCs, the dehydrogenated sample was rehydrogenated at 120 °C and $p(H_2) = 101$ bar for 16 h, and the subsequent hydrogen desorption was performed at fixed temperatures of 60, 100 and 160 °C. The hydrogen desorption curve (Fig. 4b) shows that $NaAlH_4$ with Ti-OMCs starts to release hydrogen at less than 60 °C and releases approximately 0.3 wt% hydrogen during heating to 60 °C. When the temperature is increased to 100 °C, it releases approximately 1.6 wt% hydrogen during 4.5 h, and when the temperature is further increased to 160 °C, approximately 2.15 wt% hydrogen is released. In contrast, for $NaAlH_4$ with 3 mol% TiO_2 (see Fig. S2†), no hydrogen is released under 60 °C during 3 h, and the onset temperature of $NaAlH_4$ with 3 mol% TiO_2 is approximately 100 °C. Thus, the above results indicate that $NaAlH_4$ with Ti-OMCs exhibits better hydrogen desorption kinetics than catalyzed $NaAlH_4$ at relatively low temperatures.

Fig. 5 shows the XRD patterns of the Ti-OMCs, the as-prepared melt-infiltrated $NaAlH_4$ with Ti-OMCs, and the $NaAlH_4$ with Ti-OMCs after dehydrogenation and rehydrogenation. The XRD pattern of the Ti-OMCs (Fig. 5a) shows two weak and broad peaks corresponding to the (002) and (100) planes of graphite which can be seen at 26 and 43°, respectively, indicating graphitization of a small segment of the amorphous carbon matrix at 900 °C. However, no TiO_2 is detected due to the low content in the carbon matrix. After melt infiltration with $NaAlH_4$, no diffraction line other than that of the Al is seen (Fig. 5b) suggesting that the confined $NaAlH_4$ is not crystalline and a fraction of $NaAlH_4$ decomposes to Al during melt infiltration. Moreover, the only crystalline phase detected by XRD was Al in the $NaAlH_4$ with Ti-OMCs composite after dehydrogenation or rehydrogenation (Fig. 5c and d), which may be due to the regenerated $NaAlH_4$ and its resulting NaH which are also in an amorphous state and/or highly dispersed as fine crystallites.[31]

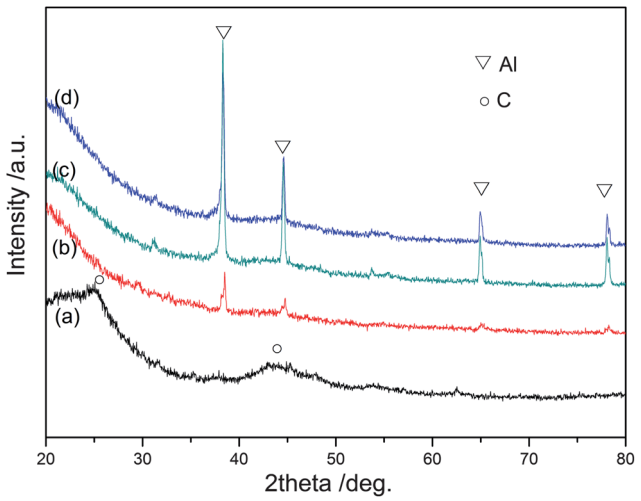

Fig. 5 XRD patterns of (a) as-prepared Ti-OMCs; (b) as-prepared melt-infiltrated $NaAlH_4$ with Ti-OMCs; (c) $NaAlH_4$ with Ti-OMCs after dehydrogenation; and (d) after rehydrogenation.

3.3. Hydrogen absorption kinetics of $NaAlH_4$ with Ti-OMCs

For technical applications, hydrogen storage materials should be able to rehydrogenate at a relatively low temperature and low hydrogen pressure. The hydrogen absorption of $NaAlH_4$ with Ti-OMCs was carried out under different conditions during eleven cycles (more details in Table 1), and the hydrogenation capacity was obtained by subsequent hydrogen desorption at 160 °C under vacuum for 150 min after rehydrogenation. Under a pressure of approximately 100 bar, the dehydrogenated samples were rehydrogenated at different temperatures for 18 h (from the 3rd to 7th cycle in Table 1). The hydrogen desorption curves of $NaAlH_4$ with Ti-OMCs (Fig. 6) show that hydrogenation capacities are 0.71, 0.99, 1.60, 1.21 and 1.77 wt% after hydrogenation at 25, 55, 83, 120 and 160 °C, respectively. The inset shows the maximum hydrogenation capacity as a function of rehydrogenation temperature, indicating that the optimum temperature of rehydrogention is 120 °C, which is in agreement with previous work.[41] However, all samples exhibit good desorption kinetics, and most hydrogen is released in 30 min. In addition, 1.61 wt% hydrogen is reversibly absorbed at a relatively

Table 1 Cycle hydrogenation test of $NaAlH_4$ with Ti-OMCs at different conditions

	Hydrogenation conditions			
Cycle	p (bar)	T (°C)	Approx. time (h)	Hydrogenation capacity (wt% H_2/$NaAlH_4$)
1	101	120	16	2.15
2	102	120	18	2.13
3	102	120	18	2.12
4	96	25	18	0.71
5	102	55	18	0.99
6	100	83	18	1.60
7	104	160	18	1.77
8	56	120	18	1.61
9	23	25	48	0.67
10	100	120	18	1.86

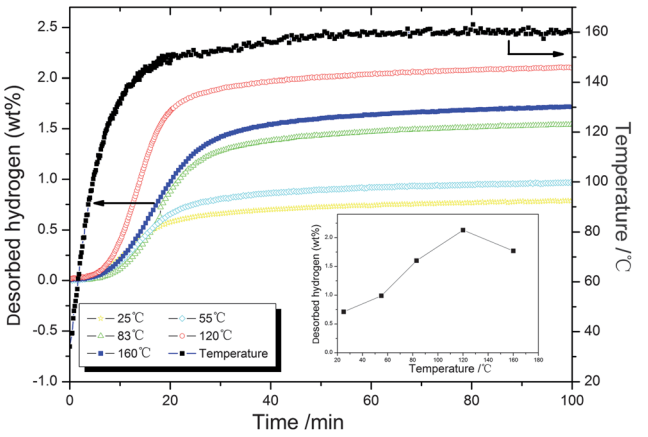

Fig. 6 Hydrogen desorption curves of $NaAlH_4$ with Ti-OMCs after hydrogenation at different temperatures. The inset shows the maximum amount of absorbed hydrogen as a function of rehydrogenation temperature.

low hydrogen pressure of 56 bar at 120 °C (8th cycle see Fig. S3†). Moreover, when the hydrogen pressure further decreases to 23 bar in the 9th cycle, the sample can still rehydrogenate approximately 0.67 wt% at room temperature (see Fig. S4†). To the best of our knowledge, these are the lowest conditions reported to date (23 bar, 25 °C) for $NaAlH_4$ hydrogenation, which may be due to the fact that both the kinetics and thermodynamics of $NaAlH_4$ are altered by the combination of nanoconfinement and catalyst addition in this method.[42]

3.4. Cycling stability of $NaAlH_4$ with Ti-OMCs

Fig. 7 shows the hydrogen desorption curves of $NaAlH_4$ with Ti-OMCs at 160 °C under vacuum for eleven cycles. Before desorption, all hydrogen absorptions were carried out at 120 °C and $p(H_2)$ = 100 bar. The curves show that about 2.31 wt% hydrogen is released in the first desorption, subsequently decreasing to approximately 2.12 and 1.86 wt% after the 4th and 11th cycle, respectively. This indicates that approximately 80% initial hydrogen is released after the 11th cycle. Thus, it can be

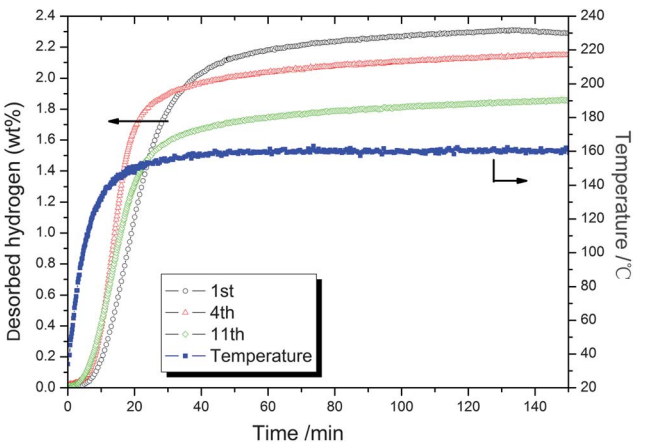

Fig. 7 Hydrogen desorption curves of $NaAlH_4$ with Ti-OMCs at 160 °C under vacuum for eleven cycles.

suggested that the hydrogen desorption capacity for $NaAlH_4$ with Ti-OMCs decreases after each further cycle, which may be due to the agglomeration of Al and/or $NaAlH_4$ nanoparticles during cycling. However, only 54% hydrogen for nanoconfined $NaAlH_4$ in an aerogel doped with 3.0 wt% $TiCl_3$ is released after the 4th cycle[34] which suggests that the $NaAlH_4$ with Ti-OMCs sample exhibits an acceptable cycling stability.

On the basis of the above observations, the results show that the hydrogen desorption kinetics, reversibility and cycling stability are all improved considerably by confining $NaAlH_4$ into the as-prepared Ti-OMCs as compared to the OMCs and ball-milled $NaAlH_4$–TiO_2 sample. However, it is found that the gravimetric hydrogen of $NaAlH_4$ with Ti-OMCs (2.31 wt%) is much lower than the theoretical value (5.6 wt%), which may be due to the decomposition of a fraction of $NaAlH_4$ during the infiltration and incomplete reversibility during the hydrogen absorption. The hydrogen storage capacity of nanoconfined $NaAlH_4$ can be increased by several methods: (1) the synthesis of mesoporous carbons with high surface area and increased pore volume; (2) increasing the hydrogen pressure to avoid the decomposition of $NaAlH_4$ during melt infiltration; (3) loading of more $NaAlH_4$ into the mesoporous carbon *via* repetitive infiltration; (4) improvement of the cycling stability.

4. Conclusions

In this study, we have reported a simple method for the synthesis of Ti-loaded high-ordered mesoporous carbons (Ti-OMCs) which can be used to combine catalyst addition and nano-confinement to improve the kinetics and reversibility of $NaAlH_4$ by melt infiltration. The Ti-OMCs were prepared *via* a solvent evaporation induced self-assembly method (EISA) followed by *in situ* crystallization and carbonation technology. The results from SAXRD, Nitrogen adsorption–desorption and TEM analysis show that the as-obtained Ti-OMCs have a well-ordered structure, uniform pore size (4 nm), and large surface area (427.9 $m^2\ g^{-1}$) and pore volume (0.34 $cm^3\ g^{-1}$). After melt infiltration, the hydrogen desorption curves show that the $NaAlH_4$ with Ti-OMCs composite exhibits better kinetics than both the catalysed $NaAlH_4$ and melt-infiltrated $NaAlH_4$ with OMCs composite. In addition, the onset temperature of the $NaAlH_4$ with Ti-OMCs composite is reduced to less than 60 °C, and 80% hydrogen is released in less than 20 min. Moreover, $NaAlH_4$ with Ti-OMCs exhibits good reversibility and cycling stability, and the optimum rehydrogention temperature is 120 °C. Furthermore, many other metal-loaded high-ordered mesoporous carbons can be synthesized in a similar fashion, for example, Ni-OMCs, Ce-OMCs and Zr-OMCs, which may be used to improve the kinetics of other complex hydrides for hydrogen storage such as $LiAlH_4$, $NaBH_4$ and $LiBH_4$ that contain a higher weight fraction of hydrogen.

Acknowledgements

This work has been financially supported by the Science and Technology Foundation of China Academy of Engineering Physics (no. 2010B0301042).

Notes and references

1 P. Jena, *J. Phys. Chem. Lett.*, 2011, **2**, 206–211.
2 B. Sakintuna, F. Lamari-Darkrim and M. Hirscher, *Int. J. Hydrogen Energy*, 2007, **32**, 1121–1140.
3 K. J. Jeon, H. R. Moon, A. M. Ruminski, B. Jiang, C. Kisielowski, R. Bardhan and J. J. Urban, *Nat. Mater.*, 2011, **10**, 286–290.
4 P. Adelhelm and P. E. de Jongh, *J. Mater. Chem.*, 2011, **21**, 2417–2427.
5 S. Orimo, Y. Nakamori, J. R. Eliseo, A. Zuettel and C. M. Jensen, *Chem. Rev.*, 2007, **107**, 4111–4132.
6 U. Eberle, M. Felderhoff and F. Schuth, *Angew. Chem., Int. Ed.*, 2009, **48**, 6608–6630.
7 N. L. Rosi, J. Eckert, M. Eddaoudi, D. T. Vodak, J. Kim, M. O. Keeffe and O. M. Yaghi, *Science*, 2003, **300**, 1127–1129.
8 J. Germain, J. M. J. Fréchet and F. N. Svec, *Small*, 2009, 51098–51111.
9 A. C. Dillon, K. M. Jones, T. A. Bekkedahl, C. H. Kiang, D. S. Bethune and M. J. Heben, *Nature*, 1997, **386**, 377–379.
10 J. Lu, Y. J. Choi, Z. Zak Fang, H. Y. Sohn and E. Roennebro, *J. Am. Chem. Soc.*, 2010, **132**, 6616–6617.
11 R. C. Bowman, C. A. Lindensmith, S. Luo, T. B. Flanagan and T. Vogt, *J. Alloys Compd.*, 2002, **330**, 271–275.
12 X. F. Liu, H. W. Langmi, S. D. Beattie, F. F. Azenwi, G. S. McGrady and C. M. Jensen, *J. Am. Chem. Soc.*, 2011, **133**, 15593–15597.
13 X. Liu, D. Peaslee, C. Z. Jost, T. F. Baumann and E. H. Majzoub, *Chem. Mater.*, 2011, **23**, 1331–1336.
14 F. Schuth, B. Bogdanovic and M. Felderhoff, *Chem. Commun.*, 2004, 2249–2258.
15 S. Orimo, Y. Nakamori, J. R. Eliseo, A. Zuttel and C. M. Jensen, *Chem. Rev.*, 2007, **107**, 4111–4132.
16 B. Bogdanovic and M. Schwickardi, *J. Alloys Compd.*, 1997, **253–254**, 1–9.
17 B. Bogdanovic, R. A. Brand, A. Marjanovic, M. Schwickardi and J. Tolle, *J. Alloys Compd.*, 2000, **302**, 36–58.
18 G. A. Lozano, C. Na Ranong, J. M. Bellosta von Colbe, R. Bormann, G. Fieg, J. Hapke and M. Dornheim, *Int. J. Hydrogen Energy*, 2010, **35**, 6763–6772.
19 G. A. Lozano, C. Na Ranong, J. M. Bellosta von Colbe, R. Bormann, G. Fieg, J. Hapke and M. Dornheim, *Int. J. Hydrogen Energy*, 2010, **35**, 7539–7546.
20 G. J. Lee, J. H. Shim, Y. W. Cho and K. S. Lee, *Int. J. Hydrogen Energy*, 2008, **33**, 3748–3753.
21 M. P. Pitt, P. E. Vullum, M. H. Sorby, D. Blanchard, M. P. Sulic, H. Emerich, M. Paskevicius, C. E. Buckley, J. Walmsley, R. Holmestad and B. C. Hauback, *J. Alloys Compd.*, 2012, **513**, 597–605.
22 R. J. Xiong, G. Sang, X. Y. Yan, G. H. Zhang, X. Q. Ye and X. L. Zhu, *Int. J. Hydrogen Energy*, 2011, **36**, 15652–15657.
23 Y. F. Liu, C. Liang, H. Zhou, M. X. Gao, H. G. Pan and Q. D. Wang, *Chem. Commun.*, 2011, **47**, 1740–1742.
24 L. Li, F. Y. Qiu, Y. P. Wang, Y. J. Wang, G. Liu, C. Yan, C. H. An, Y. N. Xu, D. W. Song, L. F. Jiao and H. T. Yuan, *J. Mater. Chem.*, 2012, **22**, 3127–3132.
25 T. J. Frankcombe, *Chem. Rev.*, 2012, **112**, 2164–2178.
26 P. Adelhelm, J. B. Gao, M. H. W. Verkuijlen, C. Rongeat, M. Herrich, P. J. M. van Bentum, O. Gutfleisch, A. P. M. Kentgens, K. P. de Jong and P. E. de Jongh, *Chem. Mater.*, 2010, **22**, 2233–2238.
27 C. P. Balde, B. P. C. Hereijgers, J. H. Bitter and K. P. de Jong, *J. Am. Chem. Soc.*, 2008, **130**, 6761–6765.
28 M. Fichtner, *Phys. Chem. Chem. Phys.*, 2011, **13**, 21186–21195.
29 M. Christian and K. F. Aguey-Zinsou, *Nanoscale*, 2010, **2**, 2587–2590.
30 S. Y. Zheng, F. Fang, G. Y. Zhou, G. R. Chen, L. Z. Ouyang, M. Zhu and D. L. Sun, *Chem. Mater.*, 2008, **20**, 3954–3958.
31 Y. Li, G. Zhou, F. Fang, X. Yu, Q. Zhang, L. Ouyang, M. Zhu and D. Sun, *Acta Mater.*, 2011, **59**, 1829–1838.
32 R. K. Bhakta, J. L. Herberg, B. Jacobs, A. Highley, R. Behrens, Jr, N. W. Ockwig, J. A. Greathouse and M. D. Allendorf, *J. Am. Chem. Soc.*, 2009, **131**, 13198–13199.
33 P. Ngene, M. H. W. Verkuijlen, Q. Zheng, J. Kragten, P. J. M. van Bentum, J. H. Bitter and P. E. de Jongh, *Faraday Discuss.*, 2011, **151**, 47–58.
34 T. K. Nielsen, M. Polanski, D. Zasada, P. Javadian, F. Besenbacher, J. Bystrzycki, J. Skibsted and T. R. Jensen, *ACS Nano*, 2011, **5**, 4056–4064.
35 R. J. Xiong, G. Sang, X. Y. Yan, G. H. Zhang, X. Q. Ye, C. L. Jiang and L. Z. Luo, *Int. J. Hydrogen Energy*, 2012, **37**, 10222–10228.

36 Y. Meng, D. Gu, F. Q. Zhang, Y. F. Shi, H. F. Yang, Z. Li, C. Z. Yu, B. Tu and D. Y. Zhao, *Angew. Chem., Int. Ed.*, 2005, **44**, 7053–7059.
37 C. H. Huang, D. Gu, D. Y. Zhao and R. A. Doong, *Chem. Mater.*, 2010, **22**, 1760–1767.
38 D. Liu, J. H. Lei, L. P. Guo and K. J. Deng, *Microporous Mesoporous Mater.*, 2011, **139**, 87–93.
39 X. Chen and S. S. Mao, *Chem. Rev.*, 2007, **107**, 2891–2959.
40 L. She, J. Li, Y. Wan, X. D. Yao, B. Tu and D. Y. Zhao, *J. Mater. Chem.*, 2011, **21**, 795–800.
41 D. L. Sun, S. S. Srinivasan, G. R. Chen and C. M. Jensen, *J. Alloys Compd.*, 2004, **373**, 265–269.
42 W. Lohstroh, A. Roth, H. Hahn and M. Fichtner, *ChemPhysChem*, 2010, **11**, 789–792.